ACADEMIC PRESS

Available online at www.sciencedirect.com
SCIENCE DIRECT®

Journal of Catalysis 219 (2003) 146–155

JOURNAL OF CATALYSIS

www.elsevier.com/locate/jcat

Physicochemical and catalytic properties of iron-doped silica—the effect of preparation and pretreatment methods

P. Decyk,[a] M. Trejda,[a] M. Ziolek,[a,*] J. Kujawa,[a] K. Głaszczka,[b] M. Bettahar,[b] S. Monteverdi,[b] and M. Mercy [b]

[a] *A. Mickiewicz University, Faculty of Chemistry, Grunwaldzka 6, PL-60-780 Poznan, Poland*
[b] *Université Henri Poincaré, Laboratoire de Catalyse Hétérogene, Faculté des Sciences, BP 239, 54506 Vandoeuvre cedex, Nancy, France*

Received 25 November 2002; revised 24 March 2003; accepted 8 April 2003

Abstract

Chemical vapor deposition (1wt% of iron) and wet and wetness impregnations (both giving Fe loading of 1.6 and 2.9 wt%) have been applied for the formation of iron-doped silica. The obtained materials were characterized by means of low-temperature N_2 adsorption, XRD, TEM, H_2-TPR, ESR, and chemisorption of CO and O_2. Their catalytic activity was tested in isopropanol decomposition and oxidation of methanol to formaldehyde. Depending on the preparation procedure various levels and strengths of Fe–silica interactions were observed. The activation conditions determine the nature of the Fe species formed. Fe^{3+} isolated species are active in isopropanol dehydration whereas Fe–oxide centers exhibit very high selectivity in methanol oxidation to methylformate and formaldehyde.

1. Introduction

Silica, besides alumina and zeolites, is often used as support for various transition metals. It has been also applied for iron oxide loading, for example, [1–3] and the obtained catalysts exhibit high activity in the gas-phase and liquid-phase oxidation processes. Among others Fe/SiO_2 catalysts have been applied for partial oxidation of methane to formaldehyde [3], or partial oxidation of hydrogen sulfide to sulfur [4–6]. Recently, they have also been successfully tested in the liquid-phase hydroxylation of phenol [2]. Depending on the reaction phase (gas or liquid), various features of the active species influence the activity and selectivity. For instance in the liquid-phase oxidation processes the strong anchoring of Fe species on the support surface is necessary to avoid leaching of the iron-active phase. Partial oxidation of hydrocarbons in the gas phase usually occurs according to a radical mechanism and therefore, a good catalyst for this process should exhibit good electron-transfer properties. It is a general agreement that the reducibility of iron-active species plays a key role in the oxidation processes. It is influenced by various factors already discussed in the literature, such as the particle size of metal or oxides, concentration of iron species, and a type of oxides formed on the support. These features depend on the preparation methods as well as the atmosphere and temperature of the pretreatment of the materials before the catalytic reaction. Therefore, in this work we have applied three various iron-supporting procedures: chemical vapor deposition (CVD), and two various impregnations (wet and wetness). The aim of our study was the estimation of iron species formed on the prepared and calcined materials and species that is generated on the iron-modified silica surface after various activation conditions. The relationship between the nature of iron species and the catalytic activity has been shown.

2. Experimentals

2.1. Preparation of the catalysts

The parent material was silica (Ventron, 99.8%). The Fe modification was carried out in three ways.

2.1.1. Wetness impregnation (denoted "imp A")

The outgassed silica (673 K, 3 h in oven) was filled in with the appropriate amount (a volume of the solution ideally equal to the pore volume of the support) of an aqueous

* Corresponding author.
E-mail address: ziolek@amu.edu.pl (M. Ziolek).

0021-9517/$ – see front matter
doi:10.1016/S0021-9517(03)00186-6

solution of iron(III) nitrate(V) and located in an evaporator flask where the catalyst was rotated and heated at 353 K for 1 h. Various concentrations of Fe^{3+} in the solution were applied due to the desired iron loading (1.6 or 2.9 wt%). The impregnated powder was dried at 393 K for 12 h and then calcined at 823 K for 4 h in an oven.

2.1.2. Wet impregnation (denoted "imp B")

The outgassed silica (673 K, 3 h in oven) was flooded with the appropriate amount (a large volume of the initial solution containing such amount of iron, which was necessary for 1.6 or 2.9 wt% Fe loading) of an aqueous solution of iron(III) nitrate(V) and shortly mixed. After that the mixture was heated at $\sim$ 353 K without stirring for 8 h. Next water was evaporated during rotation at $\sim$ 353 K for 1 h. The obtained powder was dried at 333 K for 8 h and then calcined at 823 K for 4 h in oven.

2.1.3. Chemical vapor deposition

The third type of catalysts was obtained by the chemical vapor deposition method using $FeCl_3$ as a precursor of Fe species. The CVD reaction was carried out in an apparatus built according to the literature data [7]. The silica was placed in a vertical quartz reactor and dried at 673 K for 2 h under a dry helium stream. Then the reactor was brought to 603 K. The helium stream passed through the heated container with solid $FeCl_3$. Then the system was left for 3 h at 603 K. The reaction product was cooled to room temperature and washed with distilled water for reducing the amount of chloride ions. Finally, the catalyst was dried and calcined at 823 K in air flow for 4 h.

2.2. Nitrogen adsorption/desorption

The physicochemical properties of calcined materials were studied by means of N_2 adsorption/desorption (at 77 K with a Micromeritics 2010 apparatus).

2.3. X-ray diffraction (XRD) studies

XRD patterns were recorded by TUR 42 diffractometer with Cu-K_α radiation.

2.4. TEM measurements

For TEM measurements powders were deposited on a gird with a holey carbon film and transferred to JEOL 2000 electron microscope operating at 80 kV. Scanning electron microscopy was performed using a Philips SEM 515.

2.5. Temperature-programmed reduction with hydrogen (H_2-TPR)

The temperature-programmed reduction (TPR) of the samples was carried out using H_2/Ar (10 vol%) as reductant (flow rate = 32 $cm^3\,min^{-1}$). Sample (0.025 g) was filled in a quartz tube, treated in a flow of helium at 673 K for 1 h, and cooled to room temperature (RT). It was then heated at a rate of 10 $K\,min^{-1}$ to 1300 K under the reductant mixture. A thermal conductivity detector in a PulseChemiSorb 2705 (Micromeritics) apparatus measured hydrogen consumption.

2.6. Electron spin resonance (ESR) study

The ESR investigations were carried out using a Radiopan SE/X 2547 spectrometer. A cavity operating at a frequency of 8.9 GHz (X band) was used. The ESR measurements were performed at 77 K and RT. Before the registration of spectra, the catalyst was activated under vacuum in the temperature range of RT–973 K for 2 h in each temperature (excluding RT in which only short evacuation was done).

2.7. Reduction of iron

The reduction of the catalyst was performed in a flow of hydrogen (flow rate = 50 $cm^3\,min^{-1}$). The catalyst was placed in a quartz reactor and it was heated at a rate of 10 $K\,min^{-1}$ to 673 or 973 K. The reduction at the desired temperature was performed for 2 h. In the case of CO adsorption the reduction of the catalyst was also carried out at 973 K for 4 h. After the reduction, the system was purged in helium flow for 1 h at the reduction temperature, and than the sample was cooled to RT in a flow of helium (50 $cm^3\,min^{-1}$).

2.8. Carbon monoxide chemisorption

The chemisorption of CO was performed at 253 K (the reactor was cooled with NaCl + ice mixture) on the catalysts reduced according to the procedure described above. A mixture of carbon monoxide (160.4 ppm) and helium was applied. The gas analyses were done using a GC Intersmat 120 mB equipped with a TCD detector and a column containing 13X molecular sieves, operated at 333 K. The amount of chemisorbed carbon monoxide was detected each 1.5 min. The chromatograph was connected on line with a quartz reactor filled with 0.1 g of the catalyst.

2.9. Oxygen chemisorption

The chemisorption of oxygen on the catalysts was conducted using a line described above. It was performed at 673 and 973 K. The amount of chemisorbed oxygen was detected each 1.5 min. Before the oxygen chemisorption catalysts were reduced at 973 K under the conditions described above. The oxygen adsorption on the reduced catalyst was carried out using a mixture of O_2 (101.9 ppm) and helium.

2.10. Isopropanol decomposition

Isopropanol decomposition was performed using a pulse microreactor with a helium flow of 40 $cm^3\,min^{-1}$. The cata-

lyst bed (0.05 g with a size fraction of $0.5 < Ø < 1$ mm) was first activated at 673 K for 2 h under helium flow (40 $cm^3\,min^{-1}$). The isopropanol conversion was studied in the temperature range 423–523 K using 5-µl pulses of isopropanol. Reactant and the reaction products were analyzed using a CHROM-5 gas chromatograph on line with the microreactor.

2.11. Methanol oxidation

The reaction was carried out in a fixed-bed flow reactor. The amount of 0.02 g of the catalyst, with a size fraction of $0.5 < Ø < 1$ mm, was placed in the reactor. The samples were activated in helium flow (40 $cm^3\,min^{-1}$) at 723 K for 2 h and next pretreated in a stream of O_2/He gas mixture at 723 K for 0.5 h before each run. Some experiments were carried out without O_2/He pretreatment. The reactant gas mixture of CH_3OH/O_2/He, molar ratio of $\sim 3/6/31$, was used with a total flow rate of 40 $cm^3\,min^{-1}$. The reactor effluent was analyzed using an on-line gas chromatograph (SRI 8610 GAS) with FID and TCD detectors.

3. Results

3.1. Characterization of the calcined materials

Table 1 presents the fundamental data concerning the catalysts used in this study. The surface area of the iron-doped silica changed a little upon impregnation A and B (1.6 wt%). A higher decrease of the surface area is noted for the sample containing 2.9 wt% of iron and prepared via impregnation B and for that obtained with the CVD method. It illustrates that not only the amount of Fe species but also the technique of silica doping have an influence on the surface area of the final material.

XRD study was undertaken for the estimation of phases present in the modified materials and the results are exhibited in Fig. 1. The XRD patterns of the calcined samples allow the observation of a new phase (most probably amorphous) characterized by a broad peak at $2\Theta \approx 23°$. Both samples prepared via impregnation A exhibit the presence of a new phase and lack of the XRD peaks originating from silica (Fig. 1B). This new phase results from the chemical interaction of iron with silica. It is worthy of note that the same phase is generated on the sample prepared by impregnation B (1.6 wt%) and CVD. However, in the XRD patterns of these samples a silica phase is also visible, more significantly on Fe/SiO_2 (CVD) (Fig. 1B, d).

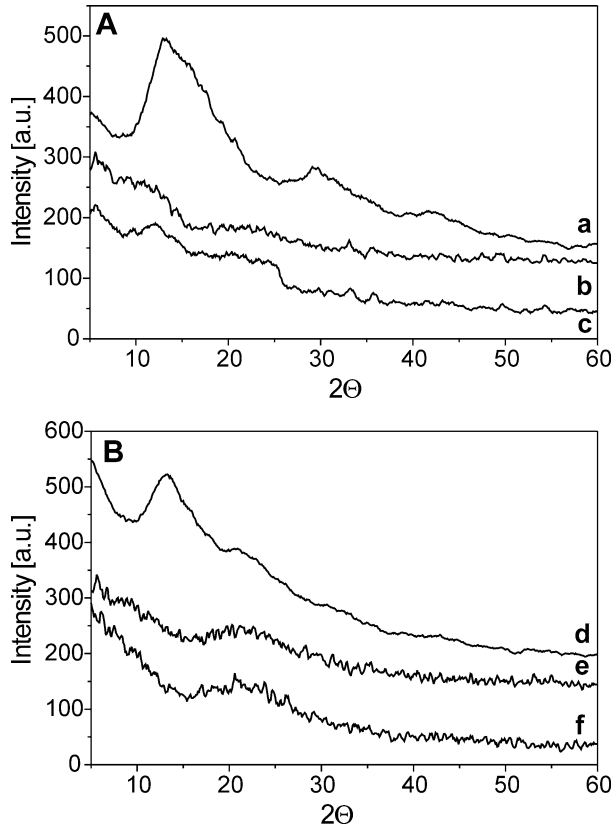

Fig. 1. XRD patterns of SiO_2 and Fe/SiO_2: (A) a, SiO_2; b, (imp B) 2.9; c, (imp B) 1.6; (B) d, (CVD); e, (imp A) 2.9; f, (imp A) 1.6.

The XRD patterns did not show other peaks, which could originate from iron oxides. However, one should remember that XRD techniques are not sensitive if the amount of the phase is too low (less than ~ 5 wt%). Moreover, if the particle size of iron oxides is very small XRD patterns cannot detect them. However, the color (red-brown) of all calcined samples clearly indicates the presence of Fe_2O_3 on the silica surface (Fe_3O_4 is black [1]).

3.2. TEM images

Transmission electron micrographs of silica impregnated with iron salt by both procedures A and B (loading of Fe 1.6 wt%) are shown in Fig. 2. It is clearly seen that wet impregnation (procedure B) leads to a better iron distribution than that obtained after wetness impregnation (A). The same phenomenon was found in the case of higher Fe loading (2.9 wt%). It is worthy of note that in procedure B the mixture of silica and aqueous solution of iron(III) nitrate(V) was kept 8 h at 353 K prior to drying. This procedure allows the liquid to penetrate into the silica pores consequently

Table 1
The characterization of the catalysts used in this study

Catalyst	Procedure of modification	Fe (wt%)	BET surface area ($m^2\,g^{-1}$)
SiO_2		0	362
Fe/SiO_2 (imp A) 1.6	Impregnation A	1.6	342
Fe/SiO_2 (imp A) 2.9	Impregnation A	2.9	345
Fe/SiO_2 (imp B) 1.6	Impregnation B	1.6	347
Fe/SiO_2 (imp B) 2.9	Impregnation B	2.9	331
Fe/SiO_2 (CVD)	Chemical vapor deposition	1.0	324

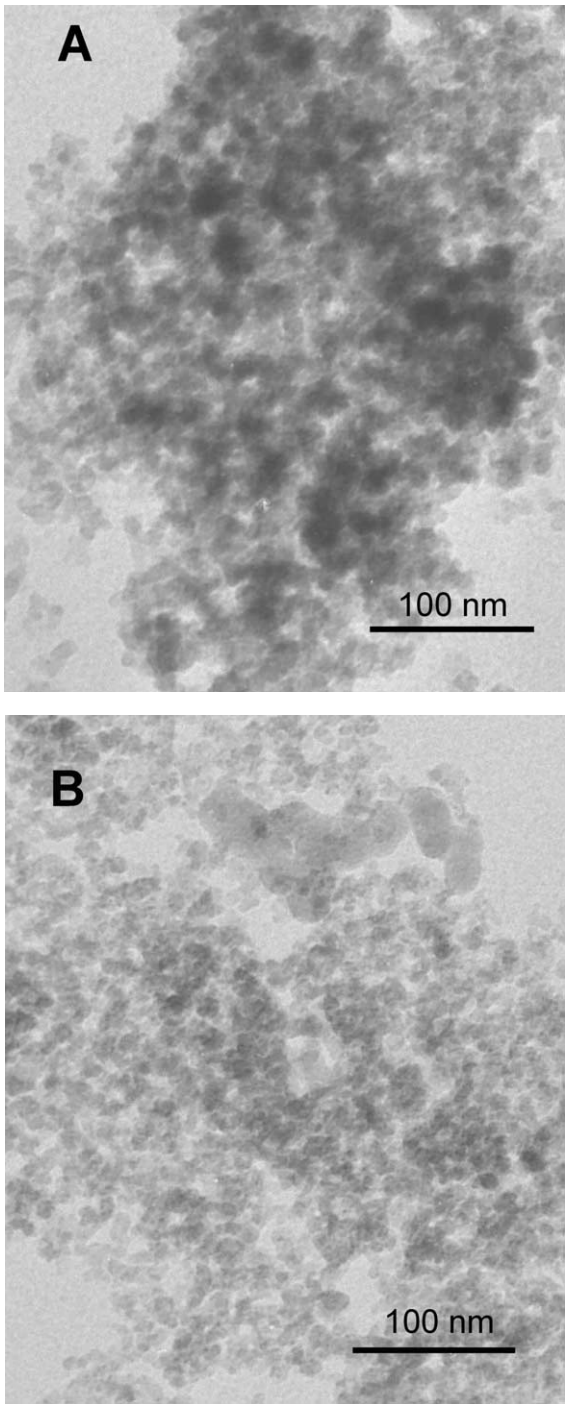

Fig. 2. TEM micrographs of Fe/SiO_2 catalysts: (A) (imp A) 1.6; (B) (imp B) 1.6.

leading to a better distribution of iron. Contrary to that, in procedure A, drying of silica wetted by $Fe(NO_3)_3$ solution was performed immediately after mixing of both phases. It caused the transport of iron around the pores of the silica particles, that in effect led to the formation of iron agglomerated species after calcination. These agglomerates can consist of Fe–oxide species or Fe–O–silica species formed as a result of a chemical reaction between iron salt and silica.

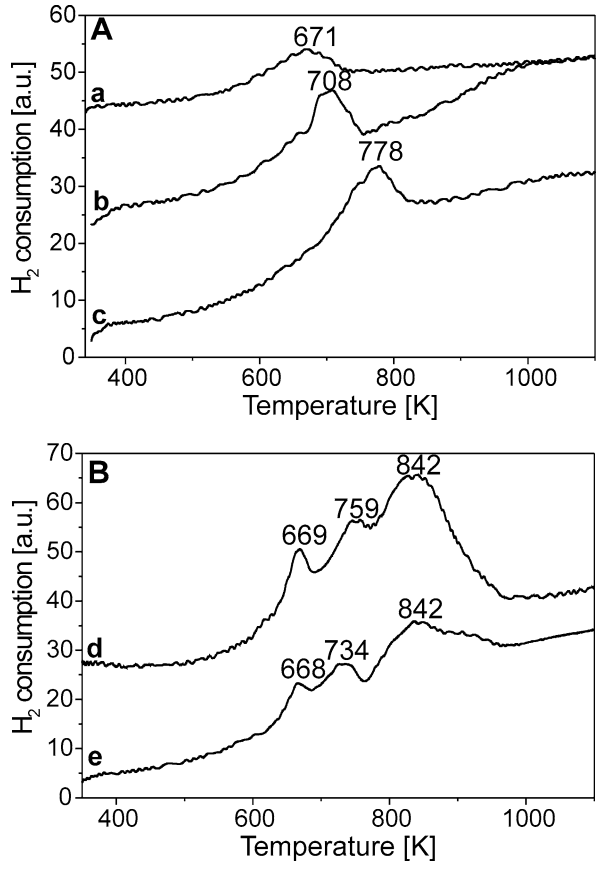

Fig. 3. H_2-TPR profiles of Fe/SiO_2 catalysts: (A) a, (imp A) 1.6; b, (imp B) 1.6; c, (CVD); (B) d, (imp B) 2.9; e, (imp A) 2.9.

3.3. H_2-TPR

Temperature-programmed reduction with hydrogen was performed after activation of the calcined samples in helium flow at 673 K. Thus, it allows the characterization of the materials pretreated under mild reducing conditions. The TPR profiles are shown in Fig. 3 and allow us to estimate the reducibility of iron species generated under the activation conditions. The reducibility of metal species has been a useful means for detecting the interactions between the metal and the support. The characteristic feature is that for a high Fe loading (2.9 wt%) three TPR peaks (Fig. 3B) are well resolved (at 669, 759, and 842 K for the imp B material and 668, 734, and 842 K for the imp A sample). The other catalysts exhibit only one TPR peak (Fig. 3A) at 671 K, 1.6 wt% (imp A) sample; 708 K, 1.6 wt% (imp B) one; and 778 K, 1 wt% CV-deposited material. The first one indicates the lowest intensity of the peak. The difference in the temperature of the peak maximum characterizes various reducibilities of metal species (a higher temperature a lower reducibility). The question arises if on all low iron-loaded samples the same iron species is formed during activation in helium flow. One can postulate that the species, which is generated after activation, is a form of iron oxide partially reduced (for instance Fe_3O_4). This species is further reduced with hydrogen only to Fe^{2+} even at temperatures as high as

1100 K and the difference in the reduction temperature for various samples allows the formulation of the following reducibility order: CVD < (imp B) 1.6 < (imp A) 1.6. The fact that iron is reduced only to ferrous cations (not to metallic form) can be explain by the stabilization of ferrous cations due to their strong interaction with the support. The same phenomenon has been described in the literature earlier for iron supported on alumina when the loading was very low (0.05%) [8,9].

In contrast, Fe/SiO_2 materials with a higher Fe loading (2.9 wt% of iron) prepared by both impregnation methods exhibit three peaks on H_2-TPR profiles as noted above. They can be assigned to the three steps of iron oxide reduction: $Fe_2O_3 \rightarrow Fe_3O_4 \rightarrow FeO \rightarrow Fe$. Such assignment is in agreement with the literature data for instance for Fe-zeolite-beta catalyst [10]. The fact that the higher loading of iron causes easier the further reduction of ferrous cations by hydrogen to metal can be understood taking into account that unsupported iron oxide can be reduced to the zero-valence state at 673 K [11]. Generally, a higher concentration of cationic species makes their reduction easier.

3.4. ESR

Mild reducing conditions are applied when the samples are activated under vacuum before ESR experiments. Therefore, the ESR spectra allow the characterization of the samples in a similar state as after activation in a helium flow. Moreover, the spectra recorded for the fresh calcined sample after a short evacuation at room temperature—shown in Fig. 4—give information about the material at the same state as that characterized by the XRD technique. In the ESR spectra presented in Fig. 4 one can distinguish two kinds of signals: (i) a broad one at $g \approx 2.1$ and (ii) a sharp signal at $g \approx 4.25$. Moreover, another less intensive signal is visible for some samples at $g \approx 6$, which is most pronounced for Fe/SiO_2 (CVD).

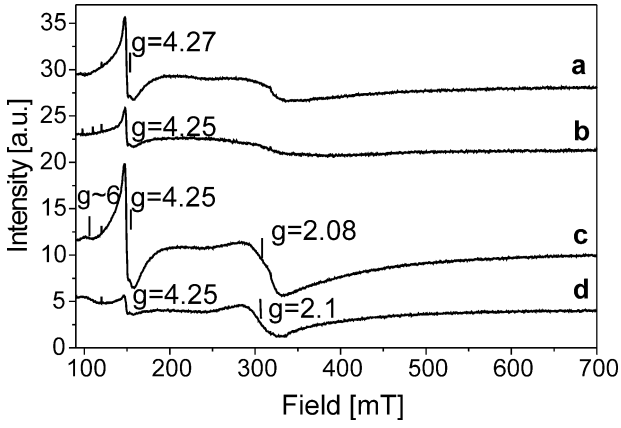

Fig. 4. ESR spectra recorded at 77 K of Fe/SiO_2 after calcination in air flow at 823 K and short evacuation at RT: a, (imp B) 1.6; b, (imp A) 1.6; c, (CVD); d, (imp B) 2.9.

There is rather an agreement in the literature (for instance [12]) that the ESR signal at $g \approx 4.25$ is typical of isolated Fe^{3+} paramagnetic cations in strong rhombic-distorted tetrahedral sites, whereas that at $g \approx 6$ can be ascribed to Fe^{3+} in the coordination of less distorted tetrahedron [12,13]. Both features are likely associated with the same isolated Fe^{3+} species. According to [3] the signal at $g \approx 6$ would correspond to particular energy transitions resulting from the resolution of the spin Hamiltonian appropriate for Fe^{3+} high-spin $3d^5$ systems. Although the discussed iron species can originate also from octahedral coordination in a rhombic-like symmetry [3] most authors describe this species to tetrahedral coordination of iron on a 3+ valence state [12–14]; the same assignment we have proposed earlier for ESR signals recorded on Fe-MCM-41 mesoporous molecular sieves [15].

A broad signal at $g \approx 2.1$ can be attributed to Fe–O–Fe species with ferri-, ferro-, and/or antiferromagnetic behavior [16]. This signal is more visible when the spectrum is scanned at RT (Figs. 5B and 6B). It can originate from various iron oxide species like γ-Fe_2O_3 or Fe_3O_4 (both ferrimagnetic), or α-Fe_2O_3 (antiferromagnetic) [1]. When the

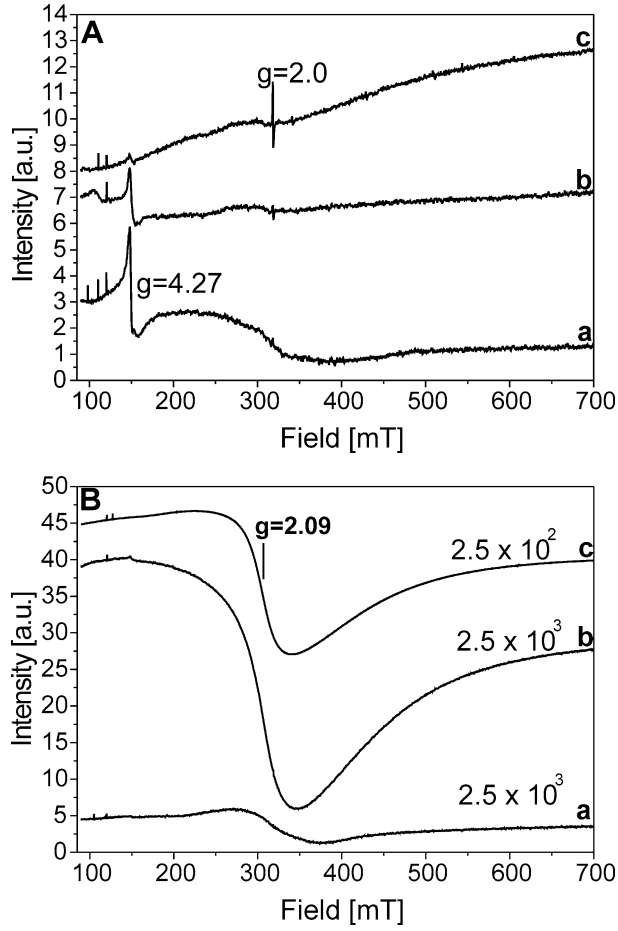

Fig. 5. ESR spectra of Fe/SiO_2 (imp A) 1.6 recorded at 77 K (A) and RT (B): a, after calcination in air flow at 823 K and short evacuation at RT; b, after evacuation at 673 K, 2 h; c, after evacuation at 923 K, 2 h.

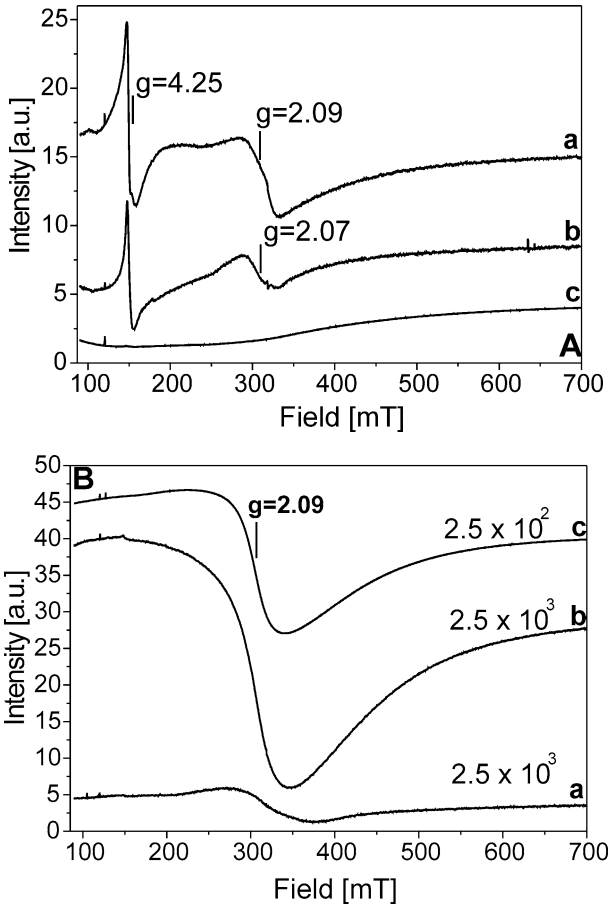

Fig. 6. ESR spectra of Fe/SiO_2 (CVD) recorded at 77 K (A) and RT (B): a, after calcination in air flow at 823 K; b, after evacuation at 673 K, 2 h; c, after evacuation at 923 K, 2 h.

spectra are recorded at RT, a great increase of the intensity of the line at $g = 2.03$ occurs, while that of the lines at $g > 3$ strongly decreases. This behavior is known and described in the literature also for other iron-containing catalysts [14].

Based on the above assignment of the ESR signals one can state that for the low Fe-loaded silica the intensity of signals due to both Fe species (isolated Fe^{3+} and Fe–oxide species) depends on the preparation procedure and changes as follows: CVD > (imp B) 1.6 > (imp A) 1.6. The ESR spectrum of impregnated silica ((imp B) with 2.9 wt% of iron—Fig. 4 spectrum d) exhibits a very low intensity of both Fe species but the ratio of the signal intensities is contrary to that for low loaded materials. The intensity of the signal at $g \approx 2.1$ is higher than that of $g \approx 4.25$ for Fe/SiO_2 (imp B) 2.9, i.e., contrary to that on the other spectra shown in Fig. 4.

All investigated samples exhibit a decrease of ESR signal intensity with increasing evacuation temperature (examples are given in Figs. 5 and 6). Two hours evacuation at 973 K causes the complete disappearance of signals from paramagnetic Fe species on Fe/SiO_2 (CVD) (Fig. 6A, c), whereas on Fe/SiO_2 (imp A) 1.6 their intensity decreases significantly. It suggests either the reduction of Fe^{3+} to Fe^{2+} or the formation of other iron ESR silent species. The presence

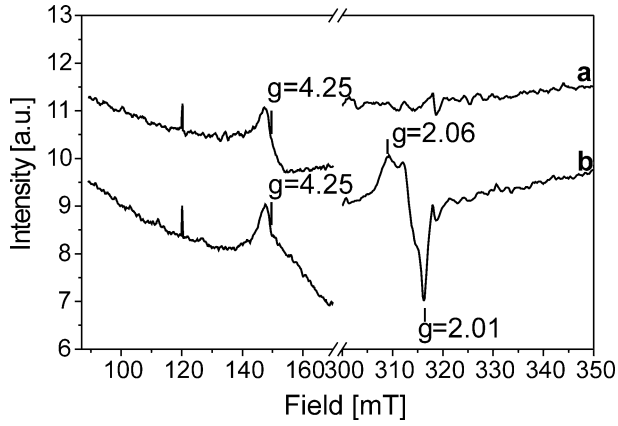

Fig. 7. ESR spectra of Fe/SiO_2 (imp A) 1.6, recorded at 77 K: a, after evacuation at 673 K, 2 h; b, after NO adsorption (1 mbar).

of Fe^{2+} cations has been documented by experiments with NO adsorption. An example of the results is given in Fig. 7 for Fe/SiO_2 (imp A) 1.6. NO was adsorbed on the sample evacuated at 673 K, i.e., partial reduced material. The paramagnetic complex $Fe^{2+}NO$ appears on the catalyst surface and is described by ESR signals (shown in Fig. 7) in the range between 300 and 350 mT. The presented signal from $Fe^{2+}NO$ seems to be a mixture of axial (characterized by $g_{\|} = 2.054$ and $g_{\perp} = 2.02$) and rhombic signals ($g_1 = 2.09$, $g_2 = 2.06$, $g_3 = 2.01$) described in the literature [17]. However, the rhombic signal dominates. These signals slowly disappear during evacuation starting from 573 K (not shown in the figure).

The reduction of Fe^{3+} to Fe^{2+} (or Fe^0) can be also concluded on the basis of ESR signals registered at RT and shown in Figs. 5B and 6B. The increasing evacuation temperature causes the growth of a broad signal at $g \approx 2.2$. It can be explained on the basis of the literature [18] by the presence of Fe^{2+} ions in combination with Fe^{3+} (as in Fe_3O_4). This is due to a change of the magnetic properties of the iron oxide/hydroxide clusters, for example, by a partial release of the near-complete cancellation of spins of antiferromagnetically coupled ions.

It is worthy of note that the increase of evacuation temperature for all calcined materials leads to the generation of a sharp signal at $g \approx 2.0$. This signal was attributed by Sachtler and co-workers [12] to superoxide ions (O_2^-) which are associated with iron ions.

3.5. CO chemisorption

Carbon monoxide is an often used adsorbate for estimation of metallic catalysts. However, it is chemisorbed in various forms on iron and other metals like nickel, palladium, ruthenium, rhodium, and platinum. CO can be dissociatively chemisorbed or associatively in various forms, linear (metal:CO = 1:1), bridged (2:1), and capped (3:1). Moreover, the formation of carbonyl species, where two or more CO molecules are bonded to a metal atom, must be

Table 2
CO chemisorption at 253 K on Fe/SiO_2 catalysts reduced with hydrogen at various temperatures

Catalyst	Fe loading		Reduction temperature (K)	CO uptake ($\mu mol\,g^{-1}$)
	(wt%)	($\mu mol\,g^{-1}$)		
Fe/SiO_2 (imp A)	1.6	285.7	673	6.8
Fe/SiO_2 (imp A)	1.6	285.7	973	100.2
Fe/SiO_2 (imp A)	2.9	517.8	673	5.6
Fe/SiO_2 (imp A)	2.9	517.8	973	6.5
Fe/SiO_2 (imp B)	1.6	285.7	673	6.8
Fe/SiO_2 (imp B)	1.6	285.7	973	73.1
Fe/SiO_2 (imp B)	2.9	517.8	673	5.4
Fe/SiO_2 (imp B)	2.9	517.8	973	24.7
Fe/SiO_2 (CVD)	1.0	178.5	673	15.5
Fe/SiO_2 (CVD)	1.0	178.5	973	139.0

considered. The relative proportions of the various forms of CO chemisorbed depend on temperature, pressure, and metal particle size [19]. Therefore, the calculation of metal dispersion is not precise and in this paper we compare CO uptake on the surfaces studied.

In this work the chemisorption of CO has been carried out at 253 K (to avoid the carbonyl formation) on the catalyst surfaces reduced with hydrogen at two temperatures, 673 and 973 K. The CO uptake is shown in Table 2.

Carbon monoxide is chemisorbed on reduced iron species (Fe^{2+} and metallic iron) [20,21]. Therefore, the CO uptake provides information about the amount of reduced iron species accessible for CO chemisorption. It must be remembered that sites below the surface cannot chemisorb CO molecules. Moreover, the steric blocking effect must be considered. The size of a CO molecule is larger than that of an iron atom, and therefore, if a CO molecule chemisorbs on a surface atom with nearest neighbors on the surface, these nearest neighbors will be sterically blocked from chemisorbing any other CO molecules [21]. It can explain the fact that a higher Fe loading leads to a lower CO uptake shown in Table 2. The reduction temperature strongly influences the CO uptake. Low Fe-loaded silica reduced at 973 K chemisorbs the higher amount of carbon monoxide than that reduced at 673 K and depending on the preparation procedure the following order of uptake can be drawn: CVD > imp A (1.6) > imp B (1.6). It was observed that the reduction time influences the CO uptake on the sample prepared via impregnation B (Table 3). It indicates that the reduction of iron oxide species is not too easy.

Table 3
The effect of the reduction (at 973 K) time on the CO uptake on Fe/SiO_2 (imp B) 1

Reduction time (h)	CO uptake ($\mu mol\,g^{-1}$)
2	73.1
4	93.1

Table 4
Oxygen uptake on the catalysts reduced with hydrogen at 973 K

Catalyst	Fe loading (wt%)	Chemisorption temperature (K)	Oxygen uptake ($\mu mol\,g^{-1}$)
Fe/SiO_2 (imp A)	1.6	673	106.6
Fe/SiO_2 (imp A)	1.6	973	119.1
Fe/SiO_2 (imp B)	1.6	673	117.9
Fe/SiO_2 (imp B)	1.6	973	145.3
Fe/SiO_2 (CVD)	1.0	673	140.5
Fe/SiO_2 (CVD)	1.0	973	194.5

It is worthy of note that the CO uptake is far from the amount of iron introduced into silica, excluding Fe/SiO_2 (CVD) reduced at 973 K. This is in agreement with the proposal of Fe location in silica (shown under Discussion) and the fact that Fe under the surface does not chemisorb CO.

3.6. O_2 chemisorption

For the chemisorption of oxygen the catalysts were reduced with hydrogen at 973 K, i.e., under conditions in which most of the iron species were reduced. The effect of the chemisorption temperature on the oxygen uptake is shown in Table 4. The highest growth in the oxygen uptake with the increase of the chemisorption temperature is noted for the catalyst prepared via CVD. The amount of oxygen chemisorbed on Fe/SiO_2 (CVD) at 973 K is even higher than Fe loading (178.5 $\mu mol\,g^{-1}$), indicating the oxygen:iron species ratio > 1. The red-brown color of all materials after oxygen chemisorption indicates the reoxidation of iron species to Fe_2O_3. This reoxidation involves two steps as concluded from two plateaus on the chemisorption curves (Fig. 8). The first step is reached very fast on Fe/SiO_2 (CVD) whereas on Fe/SiO_2 (imp B) 1.6 and Fe/SiO_2 (imp A) 1.6 it takes some time, most probably necessary for the oxygen diffusion into bulky silica–iron species.

3.7. Activity in isopropanol decomposition

The isopropanol decomposition is a test reaction for the characterization of acidic (Brønsted or Lewis) and/or basic properties [22]. Dehydration of alcohol to propene and/or diisopropyl ether requires acidic centers, whereas the dehydrogenation to acetone occurs on basic centers. Some authors [23] have stated that acetone formation takes place on redox centers.

Fig. 9 shows the influence of Fe loading on the activity in isopropanol decomposition carried out at various temperatures. The higher the iron loading the lower the conversion of isopropanol for both impregnated materials. Fe/SiO_2 (imp A) exhibits much higher activity than the sample prepared via impregnation B. The comparison of the selectivity (Table 5) for the same or similar alcohol conversion clearly shows that for a low Fe content (1.6 wt%) the selectivity is independent of the preparation procedure and acidic centers

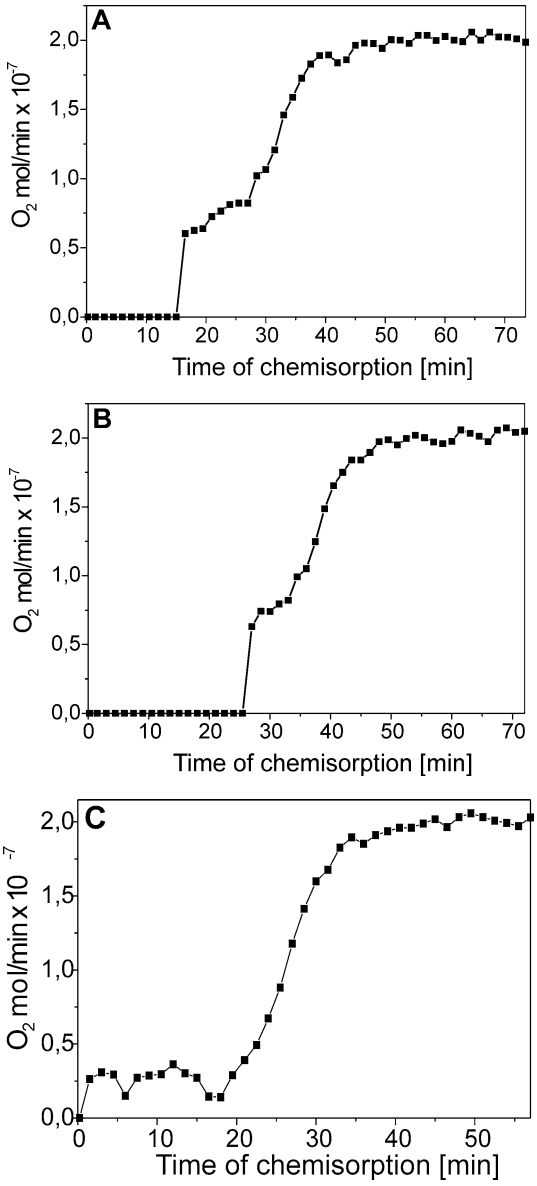

Fig. 8. The uptake of oxygen at 973 K: (A) for Fe/SiO_2 (imp A) 1.6; (B) for Fe/SiO_2 (imp B) 1.6; (C) Fe/SiO_2 (CVD).

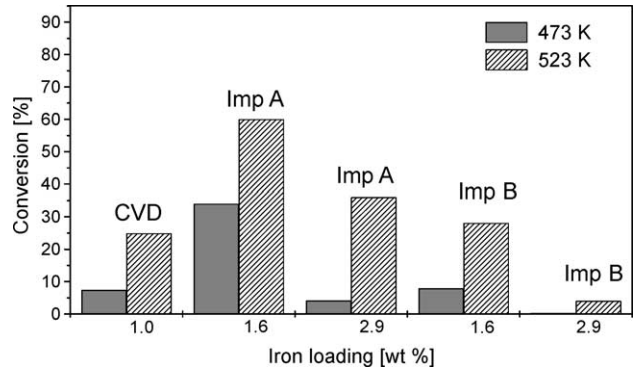

Fig. 9. The effect of iron loading on i-PrOH conversion on Fe/SiO_2.

Table 5
The selectivity of i-PrOH conversion on Fe/SiO_2 prepared via impregnation and CVD methods

Catalyst	i-PrOH conversion (%)	Temperature (K)	Selectivity (%)		
			Propene	Ether	Acetone
Fe/SiO_2 (CVD)	25	523	93	6	1
Fe/SiO_2 (imp A) 1.6	34	473	91	8	1
Fe/SiO_2 (imp B) 1.6	28	523	91	8	1
Fe/SiO_2 (imp A) 2.9	4	473	88	10	2
Fe/SiO_2 (imp B) 2.9	4	523	86	9	5

Table 6
Activity of Fe/SiO_2 catalysts in methanol oxidation at 523 K (the overall data obtained during 3 h of the reaction)

Catalyst	Methanol conversion (mol%)
Activated in O_2/He	
SiO_2	0
Fe/SiO_2 (imp A) 1.6	11
Fe/SiO_2 (imp A) 2.9	13
Fe/SiO_2 (imp B) 1.6	11
Fe/SiO_2 (imp B) 2.9	25
Fe/SiO_2 (CVD)	9
Without O_2/He activation	
Fe/SiO_2 (imp B) 1.6	6
Fe/SiO_2 (imp B) 2.9	17

are mainly active. The catalysts containing 2.9 wt% of Fe are more selective to acetone than the low-loaded materials and the acetone selectivity is higher on the material prepared via impregnation B. The catalyst obtained via the CVD technique leads to the formation of more propene than the other materials, indicating the highest acidity. The activity of this catalyst is 25% of alcohol conversion at 523 K, i.e., the lowest among the low-loaded materials.

3.8. Activity in methanol oxidation

The surface properties of the catalysts used were probed with a methanol oxidation reaction. This reaction allows discrimination between surface acid sites, formation of dimethyl ether (CH_3OCH_3), surface redox sites, formation of formaldehyde (HCHO) and methyl formate ($HCOOCH_3$) and surface basic sites, formation of $CO + CO_2$. Oxidation of methanol has already been applied for the characterization of niobium oxide catalysts modified with various components [24,25].

The overall conversion of methanol depends on the applied activation conditions and Fe loading. It was higher on the samples with a higher Fe loading. It is worthy of note that the only well-detected product was methylformate and traces of formaldehyde were registered on all the samples studied. There was no dimethyl ether and the amount of $CO + CO_2$ was negligible. Therefore, one can conclude the domination of the redox properties on the surface of all the materials used. The difference between the catalysts studied can be estimated on the basis of the methanol conversion level. The results are shown in Table 6. Contrary to the results obtained in the isopropanol decomposition, the higher

the Fe loading the higher the methanol conversion. If the catalysts prepared via wet impregnation (imp B) were not pretreated by an O_2/He mixture before the reaction, the activity of the samples was lower. It suggests the participation of Fe–oxide species as active sites in this reaction. For a low Fe loading (1.6 wt%) conversion of methanol does not depend on the preparation method, whereas a higher loading is affected by the technique of impregnation. Wet impregnation (imp B) gives rise to a higher methanol conversion.

4. Discussion

Recently, many investigations have been devoted to the characterization and catalytic use of Fe–silicalite. Depending on the desired catalytic application the location of iron in the zeolite framework can be useful or not. It is well known that Fe becomes active in oxidation reactions only after dislodgement from the framework position [26]. Taking that into account one can expect that grafting of iron species on a silica surface would be a useful method for production of active catalysts. The question arises, which form of iron species (isolated Fe ions or oxidic nanoparticles) is formed depending on the modification and activation procedure. Below we will discuss that.

On the basis of XRD results one can state that the impregnation A procedure leads to the interaction between both phases in the whole bulk whereas impregnation B left a part of silica unreacted with iron species. The smallest amount of silica interacts with iron if a CVD procedure is applied. One can propose the following scheme illustrating the formation of a new phase (dark in the scheme):

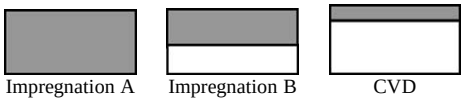

The strong iron–silica interaction occurs in the bulk silica after impregnation A, in the wide layer of a support after impregnation B, and in the narrow surface layer if the CVD procedure is used. This observation can be correlated with TEM images shown in Fig. 2. Big particles containing iron formed as a result of wetness impregnation (procedure A) can consist in a new phase resulting from iron–silica chemical interactions.

One of the important features of metal-containing catalysts is the reducibility of metal species. Therefore, in this work the effect of various activation conditions of Fe/SiO_2 catalysts on the nature of generated iron species and their reducibility has been studied. The calcined samples were activated under the reducing conditions in helium or hydrogen flow, or under vacuum at various temperatures. Activation under mild vacuum and in helium flow represents a similar reducing level, whereas hydrogen treatment gives rise to a higher reduction of iron species.

XRD patterns as well as ESR spectra recorded after short evacuation at RT allow the estimation of Fe species on the surface of calcined samples prior to the activation. The materials prepared via impregnation A exhibit the presence of a new phase characterized by a broad peak at $2\Theta = 23^\circ$ and the lack of XRD pattern from silica. It suggests the chemical reaction in bulk material between Fe–salt and SiO_2 during impregnation and calcination which leads to the formation of a mixed phase. This phase contains iron and ions originating from the support. The application of wet impregnation (procedure B) causes only a partial reaction between both phases when 1.6 wt% of iron was loaded. Part of SiO_2 does not participate in the formation of the mixed phase. The sample prepared via the CVD technique also exhibits the presence of a new phase, but in this case the domination of the XRD pattern of the support was noted. Therefore, for the material prepared via CVD of iron one can postulate the grafting of iron species on the silica surface. It is worthy of note that the new phase is more pronounced in the XRD pattern of the impregnated materials when the iron loading is lower.

The discussed new phase formed as a result of a Fe–SiO_2 chemical interaction can be correlated with the presence of Fe^{3+} species in coordination of strong rhombic-distorted tetrahedron characterized by an ESR signal at $g \approx 4.25$. This ESR signal is the most intensive one on Fe/SiO_2 (CVD), indicating that this sample has a higher concentrations of Fe^{3+} tetrahedra on the surface of a silica and iron ions do not penetrate deeper into silica (silica phase is well visible in XRD pattern). Therefore, the highest carbon oxide uptake was registered on this sample (CO is chemisorbed only on surface iron species). Both impregnation procedures gave lower concentrations of Fe^{3+} tetrahedra on a silica surface, but the lowest one was noted when the material was prepared via procedure A. The latter also exhibits a very low concentration of Fe–oxide species characterized by an ESR signal at $g = 2.1$. This phenomenon is due to a strong interaction of iron with the support. It can be concluded, similar to what Jung and Thomson [8] postulated for Fe loaded on alumina, that two types of iron oxides exist on the support: (1) strongly interacting with the support by forming solid solution with it and (2) oxides which do not interact with the support so strongly. The latter can be observed in ESR spectra. The existence of two kinds of Fe–oxide species is confirmed by two plateaus formed on oxygen chemisorption curves (Fig. 8) showing the reoxidation process. The relationship between Fe–oxide species and isolated Fe^{3+} tetrahedra determines the surface properties. The domination of Fe–oxide species over Fe^{3+} tetrahedra was observed for a higher Fe loading (2.9 wt%) on the material prepared via impregnation B.

It is worthy of note that recently [17] in ESR spectra of Fe–silicalite a single broad line centered at about $g = 2$ was assigned to hydrated iron species. However, in the materials studied in this work the discussed broad signal is still well visible after 2 h evacuation at 673 K (Fig. 6) and therefore, we ascribed it to Fe–oxide species based on [12,27].

Catalytic processes are usually performed on the activated materials. Therefore, the state of iron species on activated Fe/SiO_2 samples must be known.

Tetrahedrally coordinated Fe^{3+} ions are present in Fe_3O_4 [8]. The existence of this partially reduced Fe oxide phase (concluded from H_2-TPR and ESR results) was postulated in this work on the materials with a low iron loading activated under mild reducing conditions. During the chemical reaction with silica, Fe^{3+} in Fe_3O_4 tetrahedra is replaced by Si^{4+} and thanks to that Fe^{3+} is isolated and better visible in ESR spectra. Isolated Fe^{3+} species can be catalytically more active thanks to an easier accessibility and a stronger interaction with reagents.

The increasing evacuation temperature gives rise to a decrease of paramagnetic iron species and the formation of Fe^{2+} ions as evidenced from ESR results. Isolated iron cations represent weak Lewis acidity sufficient for the catalytic dehydration of isopropanol, but not strong enough for methanol dehydration in the presence of oxygen (the lack of dimethyl ether in the oxidation of methanol). The sequence of the activity of low Fe-loaded silica (prepared via impregnation A and B) in the isopropanol dehydration is in agreement with the reducibility of Fe^{3+} species stated on the basis of H_2-TPR results. High loaded catalysts (2.9 wt% of iron) which after mild reducing activation possess a large amount of Fe_2O_3 concluded from H_2-TPR and ESR results and less isolated Fe^{3+} species exhibit a lower dehydration activity. These catalysts represent higher oxidative properties observed in the partial oxidation of methanol. In the case of Fe/SiO_2 (CVD) the activity of Fe^{3+} isolated species is decreased by the presence of Fe–oxide forms which are not too strongly held on a silica surface. However, the highest propene selectivity obtained on this sample evidences the highest interactions of Fe^{3+} isolated ions.

On the basis of the presented characterization and the catalytic activity of Fe/SiO_2 samples one can summarize the obtained results as follows.

A 2.9 wt% of iron introduced into SiO_2 via both impregnation methods (A and B) leads to the catalysts representing easier iron reducibility, a higher amount of Fe_2O_3 and less isolated Fe^{3+}, better redox activity, and lower acidity.

A 1.6 wt% of iron introduced into SiO_2 via both impregnation methods (A and B) gives rise to the catalysts with lower iron reducibility, domination of isolated Fe^{3+} species, a lower amount of Fe_2O_3, higher acidic, and lower redox activity.

A 1 wt% of iron introduced into SiO_2 via chemical vapor deposition generated isolated, well dispersed, grafted Fe^{3+} species and Fe–oxide species weakly interacting with the support. Fe species exhibit the lowest in both reducibility and redox activity.

Acknowledgment

This work was partially supported by the Polish Research Foundation—KBN Grant 3 T09A 102 19.

References

[1] T. Ida, H. Tsuiki, A. Ueno, K. Tohji, Y. Udagawa, K. Iwai, H. Sano, J. Catal. 106 (1987) 428.
[2] Q. Liu, J. Yu, Z. Wang, P. Yang, T. Wu, React. Kinet. Catal. Lett. 73 (2001) 179.
[3] A. Parmaliana, F. Arena, F. Frusteri, A. Martinez-Arias, M. Lopez Granados, J.L.G. Fierro, Appl. Catal. A 226 (2002) 163.
[4] G.A. Bukhatiyarova, V.I. Bukhatiyarov, N.S. Sakaeva, V.V. Kaichev, B.P. Zolotovski, J. Mol. Catal. A 106 (2000) 251.
[5] M. Ziolek, I. Lasocka, I. Nowak, Polish J. Chem. 69 (1995) 1694.
[6] R.J.A.M. Terörde, P.J. van den Brink, L.M. Visser, A.J. van Dillen, Catal. Today 17 (1993) 217.
[7] T. Yashima, Catal. Surv. Jpn. 2 (1998) 121.
[8] H. Jung, W.J. Thomson, J. Catal. 128 (1991) 218.
[9] R.L. Garten, D.F. Ollis, J. Catal. 35 (1974) 232.
[10] B. Coq, M. Mauvezin, G. Delahay, S. Kieger, J. Catal. 195 (2000) 298.
[11] H. Topsøe, J.A. Dumesic, M. Boudart, J. Catal. 28 (1973) 477.
[12] H.-Y. Chen, El-M. El-Malaki, X. Wang, R.A. van Santen, W.M.H. Sachtler, J. Mol. Catal. A 162 (2000) 159.
[13] A.V. Kucherov, C.N. Montreuil, T.N. Kucherova, M. Schelef, Catal. Lett. 56 (1998) 173.
[14] El-M. El-Malaki, R.A. van Santen, W.M.H. Sachtler, J. Phys Chem. B 103 (1999) 4611.
[15] P. Decyk, M. Trejda, M. Ziolek, A. Lewandowska, Stud. Surf. Sci. Catal. 142 (2002) 1785.
[16] A. Bruckner, R. Luck, W. Wieker, B. Fahlke, H. Mehner, Zeolites 12 (1992) 380.
[17] G. Berlier, G. Spoto, S. Bordiga, G. Ricchiardi, P. Fisicaro, A. Zecchina, I. Rossetti, E. Selli, L. Forni, E. Giamello, C. Lamberti, J. Catal. 208 (2002) 64.
[18] J. Zheng, T. Schmauke, E. Roduner, J.L. Dong, Q.H. Xu, J. Mol. Catal. A 171 (2001) 181.
[19] G. Bergeretand, P. Gallezot, in: G. Ertl, H. Knozinger, J. Weitkamp (Eds.), Handbook of Heterogeneous Catalysis, Vol. 2, 1997, p. 439.
[20] M. Boudart, A. Delbouille, J.A. Dumesic, S. Khammouma, H. Topsøe, J. Catal. 37 (1975) 486.
[21] J.A. Dumesic, H. Topsøe, M. Boudart, J. Catal. 37 (1975) 513.
[22] A. Gervasisni, J. Fenyvesi, A. Auroux, Catal. Lett. 43 (1997) 219.
[23] C. Lahausse, J. Bachelier, J.C. Lavalley, H. Lauron-Pernot, A.M. Le Govic, J. Mol. Catal. 87 (1994) 329.
[24] J.-M. Jehng, A.M. Turek, I.E. Wachs, Appl. Catal. A 83 (1992) 179.
[25] X. Gao, I.E. Wachs, M.S. Wong, J.Y. Ying, J. Catal. 203 (2001) 18.
[26] A. Zecchina, G. Berlier, in: G. Centi, B. Wichterlova, A. Bell (Eds.), Catalysis by Unique Metal Ion Structures in Solid Matrices—From Science to Application, in: NATO Science Series, Vol. 13, Kluwer Academic, Dordrecht, 2001, p. 135.
[27] W.A. Carvalho, M. Wallau, U. Schuchardt, J. Mol. Catal. A 144 (1999) 91.